Req. 0.9 Bolometer FOV Chopper Scans

0.9 - A. History

Version	Date	Author(s)	Change description
0.8	2006 Nov 22	B. Ali, D. Fadda, D. Frayer, & P. Appleton	First issue
0.9	2007 Jan 10	Frayer, Ali, Fadda, Appleton, & Jacobson	Updated reduction and mosaicing

0.9 - B. Summary

We present early results of the data analysis for the FM-ILT bolometer FOV chopper scans carried out on 2006 November 15. The data were combined to make FOV maps. We estimate the size of the FOV between the calibration sources to be about 7 arcminutes on sky. We also observe evidence for a slight tilt in the FOV scans as well as a slight offset between the top and bottom blue-channel modules. The central regions of the FOV maps show excess emission that decays away from the edges of the calibrations sources, possibly suggesting the presence of scattered light from the calibration sources. Different techniques of data processing are briefly discussed.

0.9 - C. Data Reference Sheet

Table 1 shows the listing of the the data used for the analysis. To make the FOV maps, we have adopted the angular calibration of the chopper given by Klass et al. PICC-MA-TR-009, Angular Calibration of PACS FM Chopper for FM ILT tests PCD req.2.3.1, version 1.5. We have also include the results from the previous lag-based reduction (Appendix A) reported by Ali et al., FOV chopper scans, bolometer, version 0.8 for comparison.

Table 1: Summary of Data

Ref	Date	Archive filename
FOV1	15 November 2006	FILT_FOVscan_CSs_20061115_01
FOV2	15 November 2006	FILT_FOVscan_CSs_OGSEBB1_20061115_01
FOV3	15 November 2006	FILT_FOVscan_CSs_window1_20061115_01
FOV4	15 November 2006	FILT_FOVscan_CSs_window2_20061115_01
FOV5	15 November 2006	FILT_FOVscan_dark_20061115_01
FOV6	15 November 2006	FILT_FOVscan_dark_20061115_02

0.9 - D. Test Description

Table 2 shows the settings of the OGSE and internal Calibration Sources (CS) used for the tests. The tests are comprised of up-and-down scans of the full Field of View (FOV) using the internal chopper. Each data set is started at the extreme negative CPR value (-2.56×10^4) and goes to the extreme positive value (2.32×10^4), and then is repeated in the opposite direction (Fig. 1). A total of 170 steps are used with a CPR step size of 287 to cover the full FOV. The first up-and-down scan is done with the blue-short (BS) filter followed by a second up-and-down pass done with the blue-long (BL) filter. The red (R) data frames were were taken at the same time as the blue channel data, and the data were recorded at 5 Hz with 4 second exposures between chopper steps. For the dark FOV5 data, only BS and R data were taken.

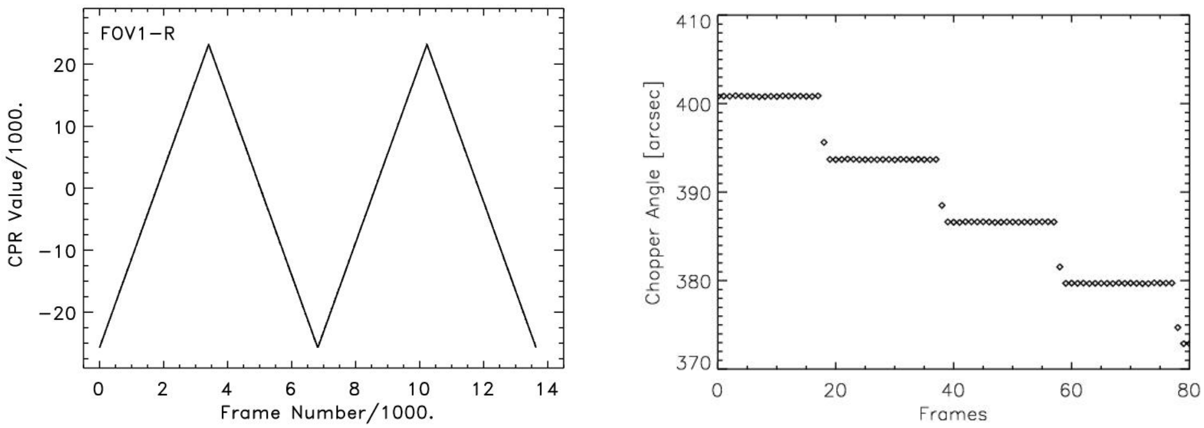

Figure 1: (Left) CPR (chopper position) as a function of readout. The first up-and-down scan set is followed by a filter change in the blue channel and the up-and-down scans are repeated. The calibration sources are observed at the large negative and large positive CPR positions. (Right) Example zoomed-in view showing the positional offset of the first frame during the chopper move. The chopper position is constant for the remaining 19 frames (4 s exposures, 5Hz sample rate).

Table 2: Test Settings

Ref	OGSE BB1_Reading (K)	OGSE BB2_Reading (K)	DM_CS1_RES_VAL (Ohm)	DM_CS2_RES_VAL (Ohm)
FOV1	5.67	5.67	79.9955	92.0024
FOV2	21.999	5.85	80.000	91.999
FOV3	22.0007	5.966	80.0020	92.0004
FOV4	22.000	5.91	79.9986	91.9979
FOV5	5.32	5.28	2.78	2.64
FOV6	5.60	5.62	1.77	1.54

0.9 - E. Data Processing

0.9 - E.1. RAW data

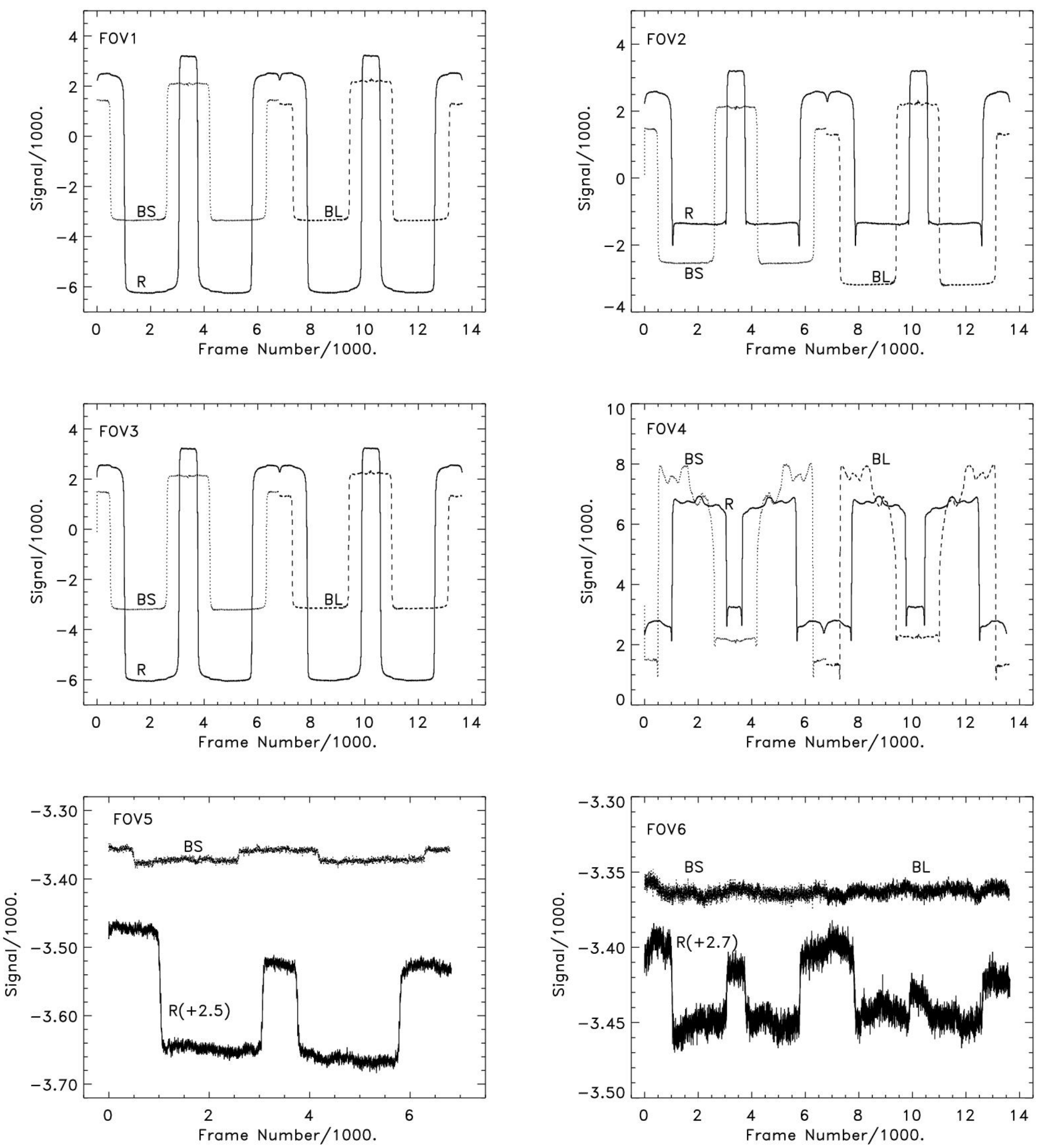

Figure 2: Raw signal as a function of time (frame number) for an example central pixel for the 6 different FOV scans (Table 1&2). Red (R) is plotted as solid lines, Blue-Short (BS) as dotted lines, and Blue-Long (BL) as dashed lines. For the FOV5 and FOV6 dark scans, the red data have been shifted up near the level of the blue dark level for comparison.

For each FOV data set listed in Table 1, we made BS, BL, and red (R) "raw" data cubes and CPR chopper angle tables. We filtered the data to include only data taken during the scans with labels 193 ("forward" direction) and 225 ("backward" direction), and did not include the small number of frames before, between, and after the scans in the analysis. The 16×16 pixel modules for the red data were transposed (see Appendix A for details) for consistency with the blue data.

For an overview of each of the FOV tests, Figure 2 shows the RAW signal as as function of frame number (time) for a central pixel of each array. The background level between the calibration sources is elevated in the FOV2 data (OGSEBB1) in comparison to the FOV1 scans. The FOV3 data (window1) is fairly similar to the FOV1 data set, with only a slight increase in the background level. The FOV4 data ("external" window2) have high background levels which are even brighter than the calibration sources and show significant structure across the window. The calibration sources were still cooling down during the dark FOV5 and FOV6 scans, as shown by the decay of the observed calibration signal as a function of time. The calibration signal is visible for both the blue and red channels in FOV5 and for the red channel in FOV6. The observed "edges" of the calibration sources are not perfectly sharp and some "scattered light" from the calibration sources is visible. For example in FOV1 and FOV3 red data sets (Fig. 2), the decay from edge of the brighter calibration source (at large CPR values) is readily apparent.

0.9 - E.2. Data Reduction

Normal photometry data are planned to be taken in chop-mode with "on-off" pairs which should remove a significant fraction of the instrumental signatures. The FOV data were taken by simply stepping the chopper position through the full range of motion so the standard "on-off" pair reduction is not possible. The initial analysis at the NHSC used a lag-based reduction technique (Appendix A). A lag-based approach may be more applicable for observations scanning at a constant rate than for these chopper-step observations. For the analysis here, we employed a simple reduction technique where the Basic Calibrated Data (BCD) frame is given by:

$$BCD = (RAW - DARK)/FLAT, \tag{1}$$

where the DARK represents the detector-to-detector offsets ("dark" and bias signal) and the FLAT represents the relative detector-to-detector gains. This approach works best if the the offsets and gains do not vary significantly as a function of time. This assumption is generally not the case for bolometers, but the PACS bolometers are well enough behaved such that this simple approach is sufficient for these analysis (the adoption of this technique is by no means an endorsement of this approach). We also briefly looked at taking a median of the frames at the same chopper position to make the BCD (e.g., combine the 19 frames at same position, see Figure 1 (right)). The reduction of an example frame is shown in Figure 3.

A "global" DARK for each filter was derived from the dark FOV6 data. For each detector, the median of the signal of the RAW data cube was taken over all of the frames to give the DARK value. "Self-calibration" DARKs were also made for the darker regions of the background frames between the calibration sources for comparison (e.g., as shown for FOV1-BS throughout this report).

The FLATS were derived from the bright calibration source data. After subtracting the DARK frame from the RAW cube, the signal for each detector was derived by taking a median of all values seeing a calibration source (CS). The resulting signals for the detectors were then normalized by the median over the array to yield a normalized FLAT. FLATS were made for both calibration sources when possible. For the current analysis, we have adopted an average FLAT made from FOV1 data.

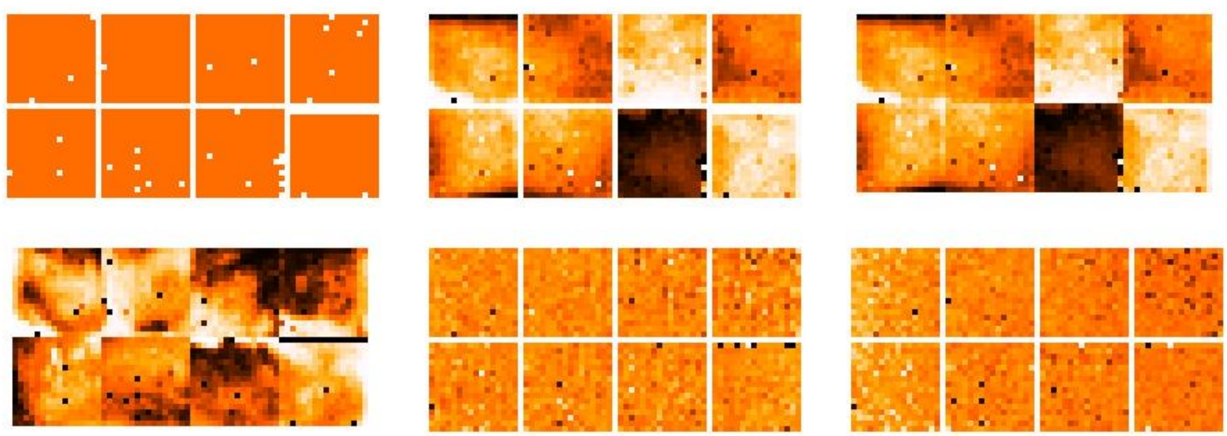

Figure 3: Example FOV1-BS frame through the reduction steps. Starting from top-left corner and going clockwise: (a) the pixel mask file where good pixels are shown in color, (b) the RAW data frame, (c) the DARK/offset frame, (d) the FLAT/gain frame, (e) the BCD frame, and (f) the co-addition of the frames at the same chopper-position. The DARK and FLAT frames do not include the extra pixel space between the modules.

0.9 - E.3. Data Co-addition and FOV Mosaics

Several different techniques of combining the FOV data have been used to make mosaics of the FOV data to determine the advantages and limitations of mosaicing software with PACS data.

0.9 - E.3.1. JIDE

Figure 4: The FOV maps for the Blue Short filter using the lag-based reduction.

Initial mosaics of the FOV data were made with JIDE using a lag-based reduction technique (Appendix A). Only data within the first scan pass from the negative CS to the positive CS were used in making mosaics for the lag-based reduction. The data were co-added to the nearest pixel using the calculated array shifts along the x-axis based on the chopper calibration. Figures 4– 6 show the mosaiced FOV maps for the six files adopting the lag-based row reduction. The maps (including the dark frames) show "banding"/"stripes" across the scan direction. This is expected given that the differences in the gain and offset values for the pixels in the reference columns manifest themselves as the "stripes" along rows in the mosaics. The maps for the blue filters are very similar while the red channel maps appear as mirror images of the blue channel for these reductions.

Figure 5: The FOV maps for the Blue Long filter using the lag-based reduction.

Figure 6: The FOV maps for the Red filter using the lag-based reduction.

0.9 - E.3.2. MOPEX

MOPEX is the mosaicing software used for Spitzer data. It allows for accurate sub-pixel interpolation, the application of distortion corrections, and has several options for carrying-out outlier rejection. For the FOV data, MOPEX gives similar results as the simple nearest-pixel JIDE co-addition. For the MOPEX co-addition, we assumed exactly one pixel space between each of the modules for the blue and red channels. The frames were given RA and Dec positions using the chopper angular calibration report. The RA=0.0 and Dec=0.0 position corresponds to the exact center of the array (in the space between the modules) when the CPR value is zero. We adopted a convention where negative CPR values correspond to negative RA values (west), and positive CPR values correspond to positive RA values (east). We used $2''$ output pixels for the blue channel and $4''$ pixels for the red channel. In addition to the mosaic, MOPEX also makes an empirical noise image based on the rms of the pixel stack and a coverage map giving the number of observations per point on the sky (Fig. 7).

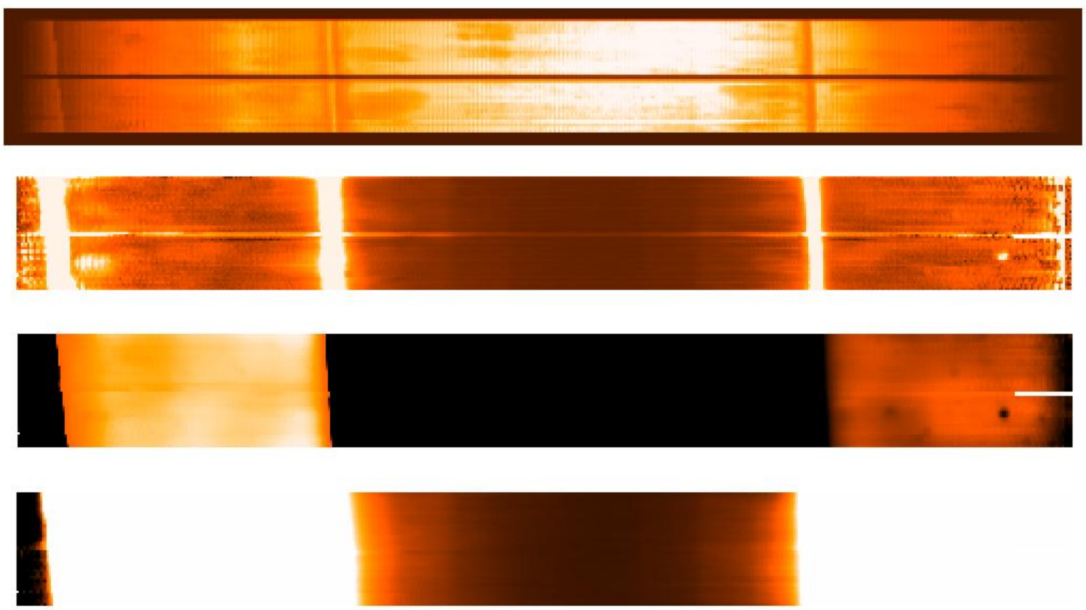

Figure 7: MOPEX products for the FOV1-BS map. From top to bottom: (a) the coverage map, (b) the std noise map, (c) the mosaic with a stretch showing the right (western) calibration source, and (d) the mosaic with a stretch showing the center region between the calibration sources. This reduction was done using a FLAT and DARK made from this data set ("self-calibration").

Figures 8&9 show the mosaics of the RAW and DARK(global)+FLAT reduction of the FOV1 data. The distance between the calibration sources is significantly larger for the red channel than for the blue channel. However, this may have resulted from the improper re-arrangement of the red data before co-addition. We followed the prescription previously done for lag-based reduction of one scan pass (Appendix A) which may not be applicable in general for the red data taken in both scan directions (e.g., we may have made a "minus" sign error in the orientation of the red modules [TBR][1]). Given the questions regarding the co-addition of the red data, we limit the discussion of the results to the blue-channel data.

[1] TBR is To Be Resolved, and TBD is To Be Determined.

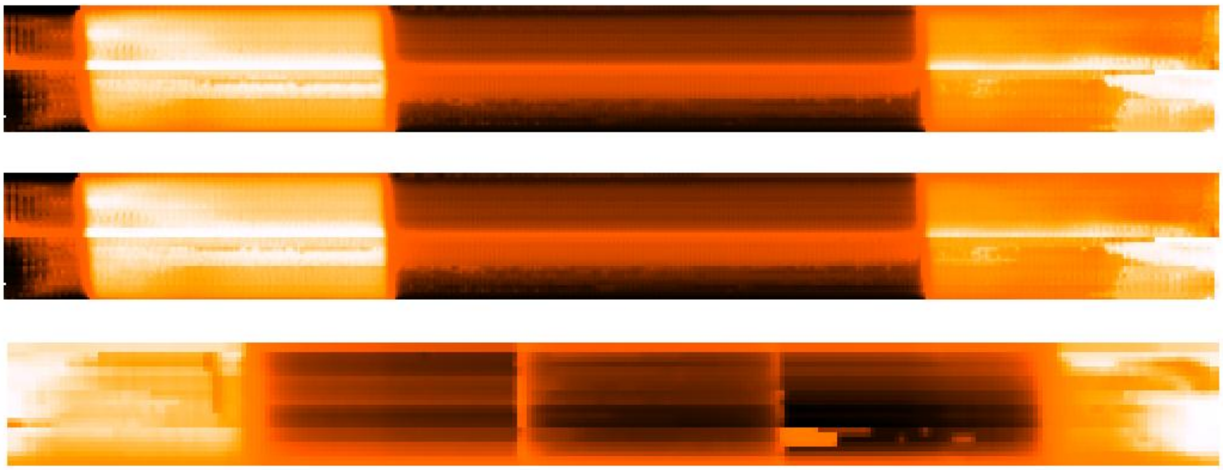

Figure 8: MOPEX mosaics for the raw FOV1 data: BS (top), BL (middle), and R (bottom). The data have been aligned to the same WCS coordinate system. The red modules may have been improperly re-arranged before co-addition (TBR).

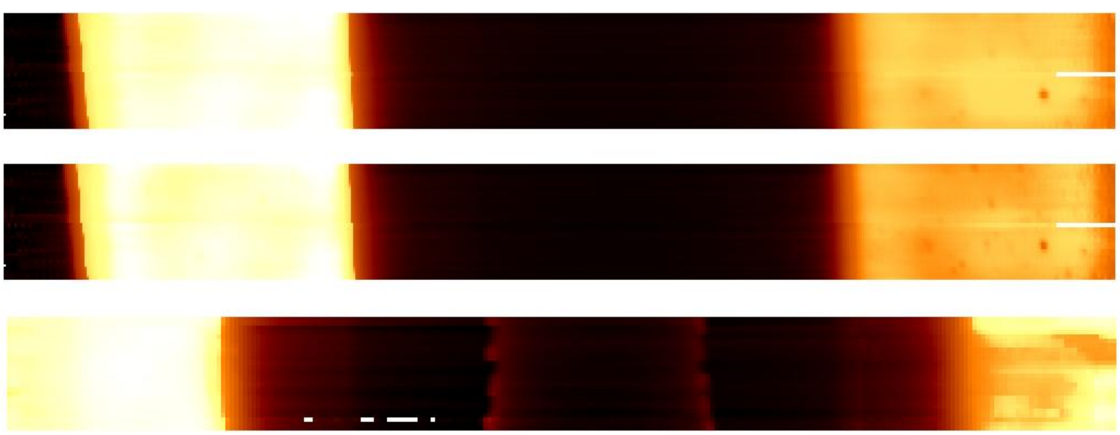

Figure 9: MOPEX mosaics for the FLAT+DARK(global) reduction of the FOV1 data shown in Figure 8: BS (top), BL (middle), and R (bottom) data. The stretch was chosen to show the spots in the right (west) CS for the blue channel.

0.9 - E.3.3. CM

CM was designed for Boomerang CMB map making by Brendan Crill (IPAC). CM works with time-ordered data and iteratively solves for the sky and noise; similar to MADmap, but assumes that the noise covariance matrix only depends on the time lags which significantly speeds up the processing. The current CM filter does not handle large, sharp jumps in the data very well. For the FOV data, the CM solutions significantly overshoot at the edges of the calibration sources (Fig. 10). Similar "ringing" artifacts were reported by the SPIRE team for SPIRE simulations scanning across bright sources. Modification of the CM code would be needed to mitigate these effects.

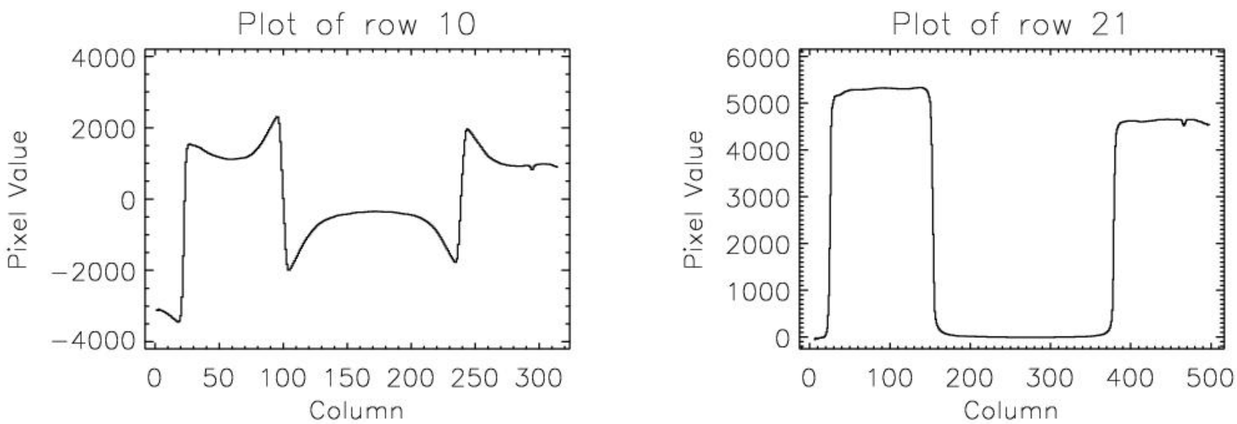

Figure 10: (Left) Plot along the row with dark spot in the FOV1-BS data using CM which shows the "ringing" artifacts at edges of calibration sources. For comparison, a similar row passing through the dark spot using the self-calibration(DARK+FLAT)+MOPEX reduction is shown at the right.

0.9 - E.3.4. MADMap

MADMap is widely used for CMB map making and has been adopted by the SPIRE team for their planned map making (Clements et al., Sept. 2006, SPIRE Mapmaking Algorithm Review Report). It has recently been compiled at the NHSC, and its use with PACS data is under investigation (MADMap FOV results, TBD).

0.9 - F. Results

The FOV maps show evidence for a slight tilt in the chopping direction of about 2° as determined from the observed slant of the edge of the calibration sources. The tilt appears to get larger at the extreme positive CPR values (towards the left/east in the maps). In addition, the upper blue modules appear to be shifted by about 2–3 arcsec left with respect to the lower blue modules, as evidenced by the apparent jump of about 1 pixel in the middle of the blue maps (e.g., Fig.9).

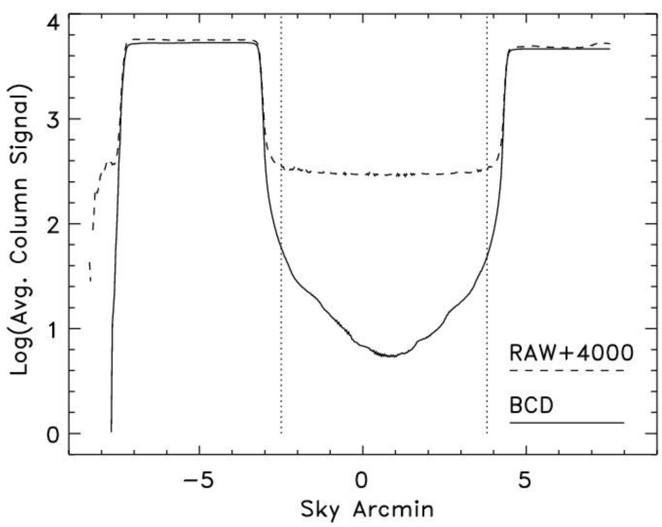

Figure 11: Averaged signal for each column in the FOV1-BS mosaic as a function of sky arcmin. The DARK(global)+FLAT BCD reduction is shown as the solid line, and the RAW data is shifted up by 4000 DN for comparison (dashed-line). Inside the dotted lines represents the region where the BCD signal is less than 1% of the signal from the calibration sources.

We measured the location of the CS edges from the blue-channel maps. Figure 11 shows a cut along the mosaic made by averaging the data for each column of the FOV1-BS1 mosaic. The measured separation between the inner-edges of calibration sources is 7.7 ± 0.2 arcmin (Table 3). The signal from the calibration sources appears to bleed/scatter into the central regions. Figure 11 shows the decay of the signal from the calibration source edges into the central regions. The observed low point of FOV1-BS signal is about 5 DN above the global DARK value derived from the FOV6-BS dark data. Some fraction of this excess may be due to presence of weak latents from the calibration sources or systematic gradients in the FLAT-fielding process and/or DARK subtraction [TBR]. Initial analysis does not seem to show stronger signals in the data as detectors fall away from the CS in comparison to when the detectors move onto the CS, suggesting that latents may not be a significant issue. The excess signal in the central regions may represent scattered light detected from the CS within the dark FM-ILT testing environment. In flight, with a warm telescope, these effects may be negligible [TBD].

Table 4 shows the measured sensitivity for the different types of data processing. The sensitivity measurements were made by computing the standard deviation within the central regions between the calibration sources for the FOV1-BS mosaics. The FLAT/gain corrections were normalized to 1, so that the data are in raw DN units. By correcting for the relative offsets and gains of the detectors, we improved the resulting rms dispersion by about 2 orders of magnitude. The lag-based reduction does not improve the noise in the maps due to banding. CM processing improves the noise properties of the data, neglecting the artifacts from the bright edges. By making DARK/offset corrections from the same data set ("self-calibration"), the sensitivity is improved by more than a factor of two in comparison to using a global DARK file made from separate DARK observations.

Table 3: FOV Measurements

Location	Left (E), Right (W) Sky Coordinates [arcmin, arcmin]	Size of Window [arcmin]
Inner CS edges	3.25E, 4.45W	7.7
5% of CS level	2.95E, 4.20W	7.15
1% of CS level	2.50E, 3.80W	6.3

Table notes – Measurements for the FOV1-BS mosaic with respect to the center of the array when the CPR value is zero.

This may imply that the time variations of the detector offsets are important (and that chopped photometry observations would yield better results). We also compared the results of taking the median of the frames at the same position before co-addition within MOPEX and find a slightly lower rms value; however this may reflect, to some degree, a change in calibration (i.e., systematic scaling differences between taking a median of the frames versus the averaging of frames as done by MOPEX [TBR]).

Table 4: Sensitivity Measurements

Data Type	RMS (1σ) [DN]
RAW data	283.2
Lag-based reduction	303.8
RAW data + CM processing	79.1
Lag-based reduction + CM processing	93.3
Global-DARK+FLAT reduction	3.7
Self-Cal DARK+FLAT reduction	1.4
Median of frames at same position and self-Cal DARK+FLAT reduction	1.3

0.9 - G. Conclusions

We estimate a FOV of about 7 arcminutes on sky which is consistent with expectations from the optical model. We observe evidence for a slight tilt in the FOV scans as well as a slight offset between the top and bottom modules for the blue channel. We detect excess signal in between the calibration sources with respect to the DARK level when the calibration sources were turned off. The signal appears to decay away from the edges of the calibration sources into the central regions which may indicate possible scattered light issues.

Most of the analysis has been done on the FOV1-BS data. We still need to sort out potential orientation issues with the red data [TBR]. In principle, these FOV data could be used to measure the stability of the offsets and gains [TBD] which may be helpful for refining the optimal approach for PACS data reduction. Long-term, different methods of mosaicing will be tested with the FOV data.

0.9 - H. Appendix A: Lag-Based Reduction Procedure

The lag-based reduction was the reduction technique used for previous versions of the NHSC FOV reports. This analysis only include data from first leg of the scans from maximum negative CPR values to maximum positive CPR values, and not the full 4 scan passes shown in Figure 1 (left). The following is taken from v0.8 of the report.

The lag-based reduction procedure used here is relatively simple and follows these steps:

1. Remove gain variations across pixels. This is a multiplicative effect and must be corrected in order to properly co-add signals.
2. Remove offset variations present in the detector pixels. This is an additive effect and must be removed in order to properly co-add signals.
3. Shift and Co-add individual frames/images at each chopper position (mosaicing).

0.9 - H.1. Step 1. Determination of gain and offset variations.

The analysis is based on the fact that the time series of each pixel is in essence a scan of the FOV. Figure 12 shows this behavior for data file 1 (FILT_FOVscan_CSs_20061115_01). Across array lines, the signal seen by one pixel in the same row will eventually be seen by another pixel in the same row. The exceptions are the coverage gaps at the edges of the FOV. We must also make the following assumptions:

Assumption 1: That the 1/f noise averages to 0.

Assumption 2: That the “tilt” between the detector axis and the long-axis of the FOV is negligible.

Within those assumptions, one can relate the signal between two pixels (on the same row) as:

$$S_1(t) = S_2(t + \Delta t) * g_{1,2} + \Delta O_{1,2} \tag{2}$$

where,
S_i is the signal in pixel i.
t is time.
$g_{1,2}$ is the relative gain between pixel 1 and 2, and
$\Delta O_{1,2}$ is the relative difference in offset values between the pixels.

The parameter g describes both the optical flatfield and responsivity variations (both are multiplicative quantities). Thus, one can simply determine the values for g, and O by relating the two signals together and fitting a linear model to this relation. In the resulting fit, the intercept gives the value of O, and the slope gives the value of g. The lag, $t + \Delta t$ is the difference in frames/time when the same signal is seen between the two pixels and is determined via a simple cross-correlation of the two signals. In practice, we determined the lag values for each column and find that this lag is satisfactorily described by a 3^{rd} order polynomial. Figure 13 illustrates the lag and the fit to the lag.

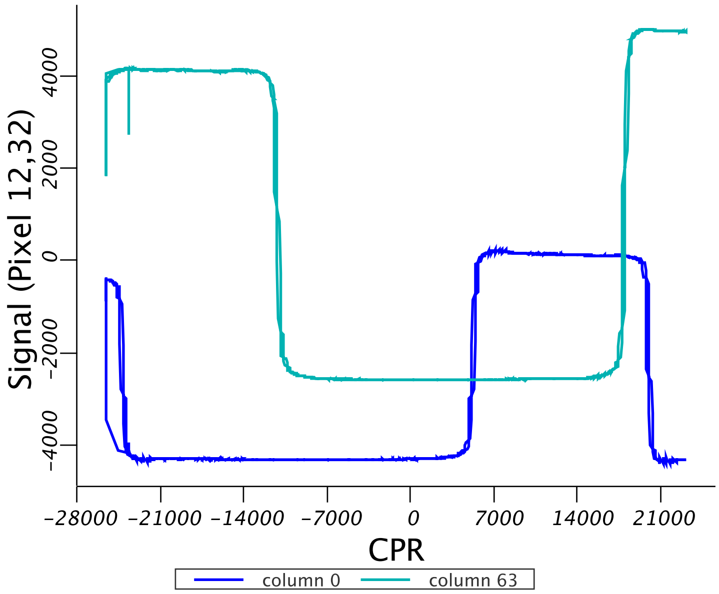

Figure 12: The signal as a function of chopper position for the leading (column 63) and trailing (column 0) edges of the blue array. The chopper scan starts at the extreme negative end of the CPR range and progresses to the extreme positive values. The high plateaus in the pixel signal are the two calibration sources.

To carry out this analysis, we chose column 12, arbitrarily, as the reference column. The remaining columns are offset-ed and scaled (as described above) to the pixels in this column.

To further simply the analysis (for "quicker" results), we also considered only one direction for the scan (up) only. This meant that the lags need only be determined for one scan direction. We used the LBL and WPR header values To obtain this sub-section of the data. For the blue channel this is all data with LBL=193. For the red channel, this is all data with LBL=193 and WPR=0.

The gain and offset values determined in this way are only relative to the chosen reference pixel.

0.9 - H.2. Step 2: Mosaicing

Each frame/image in the data cube samples a different part of the PACS FOV. The creation of the final mosaiced image requires shifting and co-adding the individual images to stitch together the final map of the FOV. The magnitude of the shift is determined by the CPR value of the frame and the chopper calibration.

The shifts are given by the following relationship:

$$Shift(\text{pixels}) = \text{Chopper Throw in arcseconds(CPR)}/Magnification/PFOV \tag{3}$$

Where the Chopper Throw in arcseconds (as a function of CPR) is from the chopper calibration curves (PICC-MA-TR-009).
$Magnification$ is 80.69 arc-seconds (also from PICC-MA-TR-009), and

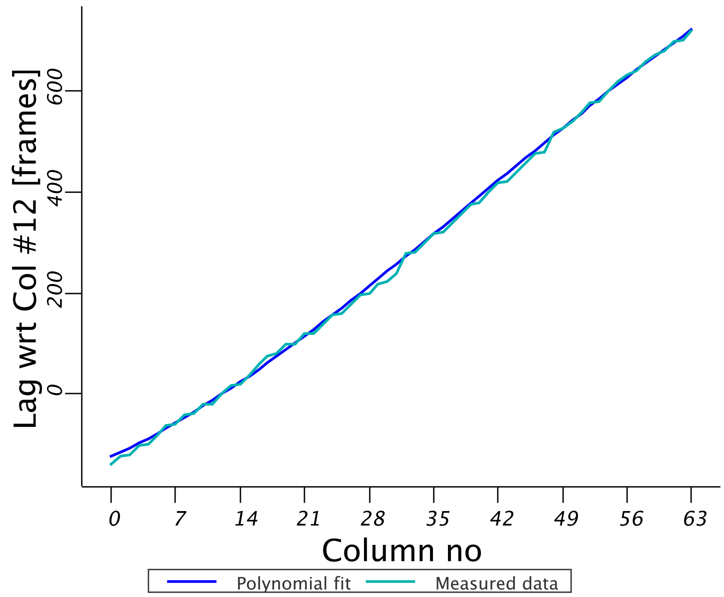

Figure 13: The lag (in frames) between column 0 (ignore y-label) and subsequent columns of the array. We find that a 3rd order polynomial (shown in blue) adequately describes the lag.

$PFOV$ is the pixel field of view. We used 3.2"/pix and 6.4"/pix for the blue and red arrays, respectively. The shifts are further rounded to the nearest pixel (integer values). The sense of the shift here is in the opposite direction to the detector X-axis (across columns).

Assumption 3: That the inter-module space (about 1 pixel) can be neglected. Neglecting this inter-module space smears the data slightly; However, making this assumption saved CPU and memory cycles to add space to each of the several thousand individual images.

The masked/dead pixels, as given by the calibration file *PacsCal_PhotBadPixelsMask_FM_1_0.fits*, are ignored.

For the red channel (band="R"), we further noticed that the arrays are flipped about the inter-module space in the sense that rows 0:15 of the first red module (first 16 columns) see the data after the 2nd module. We accounted for this by transposing the array as follows (in JIDE syntax):

$$cube[:,:16,:] = signal[:,16:,:] \quad (4)$$

$$cube[:,16:,:] = signal[:,:16,:] \quad (5)$$

Where, *signal*, is the original data cube extracted from the decompressed Frames object containing the red channel data, and *cube* is the transposed data cube. All subsequent analysis is carried out on *cube* array.